NANO LETTERS

2008
Vol. 8, No. 8
2490-2496

Coalescence and Interface Diffusion in Linear CdTe/CdSe/CdTe Heterojunction Nanorods

Bonil Koo and Brian A. Korgel*

Department of Chemical Engineering, Center for Nano- and Molecular Science and Technology, and Texas Materials Institute, The University of Texas at Austin, Austin, Texas 78712-1062

Received May 27, 2008; Revised Manuscript Received June 26, 2008

ABSTRACT

Colloidal nanorods with linear CdTe/CdSe/CdTe heterojunctions were synthesized by sequential reactant injection. After CdTe deposition at the ends of initially formed CdSe nanorods, continued heating in solution leads to Se−Te interdiffusion across the heterojunctions and coalescence to decreased aspect ratio. The Se−Te interdiffusion rates were measured by mapping the composition profile using nanobeam energy dispersive X-ray spectroscopy (EDS) along the lengths of individual nanorods aged in hot solvent for different amounts of time. The rate of nanorod coalescence was also measured and compared to model predictions using a continuum viscous flow model, which appears to provide a reasonable estimate of the coalescence rate.

Colloidal chemical routes can be used to synthesize relatively complicated heterojunction nanostructures, such as multiple quantum well quantum dots with onionlike shell structures,[1–4] linear heterojunctions in quantum-size rods[5–9] and branched structures like tetrapods,[5,10,11] and even "superlattice" quantum wells with oscillating composition along the lengths of nanowires.[12] Heterojunctions create built-in electric fields that deplete or accumulate electrons and holes within the nanostructure, which is potentially useful for optoelectronic technologies like light-emitting diodes,[13] photovoltaics,[14] and optical sensors.[15] The large surface area-to-volume ratio of colloidal nanocrystals and nanorods helps relieve strain at epitaxial interfaces between materials with large lattice mismatches to alleviate the formation of extended defects.[2,16–18] These interfaces, however, can restructure in relatively short times with atomic interdiffusion across the heterojunctions.[6–8,19–21] Furthermore, nonspherical nanocrystals can coalesce into spheres.[6–8,22,23] The dynamics of these processes requires further study and better understanding.

In this letter, the rates of heterojunction interdiffusion and coalescence of CdTe/CdSe/CdTe nanorods are reported and compared to model predictions. The Se and Te composition profiles were mapped in individual nanorods aged in hot solvents for different amounts of time to determine the Te in CdSe diffusion coefficient and evaluate the influence of strain on the interdiffusion rates across the heterojunctions. The measured rod-to-sphere coalescence rates were compared to rates predicted using a continuum viscous flow model for nanorod-to-sphere coalescence. Se and Te interdiffusion rates appear to be independent of strain at the CdSe/CdTe interface and the continuum model gives a reasonable approximation to the measured coalescence rates.

Linear CdTe/CdSe/CdTe heterojunction nanorods were synthesized by high-temperature arrested precipitation using a sequential reactant injection method.[6,24] (See Supporting Information for Experimental Details.) In this procedure, CdSe nanorods first precipitate in an initial reaction step, followed by a subsequent controlled heterogeneous deposition of CdTe at the tips of the CdSe nanorods. Figure 1 shows transmission electron microscopy (TEM) images of a nanorod sample imaged at different times during a preparation. The initial CdSe nanorods (Figure 1a) have an initial average diameter and length of 4.2 and 19.6 nm. Immediately after adding Te-TOP, the nanorods grew by 2.5 nm on each end to 24.6 nm (Figure 1b). The nanorod diameter also increased slightly to 4.7 nm (by 0.5 nm), which corresponds to the adsorption of approximately one CdTe monolayer. The nanorods are wurtzite crystals elongated in the (hexagonal) [001] crystallographic direction (see XRD data in Supporting Information) and the linear deposition of CdTe on the polar CdSe (and CdTe) (001) surfaces (i.e., the ends of the nanorods) is approximately 10 times faster than the deposition on the nonpolar sidewall surfaces.

The nanorods coalesce to shorter aspect ratios if they remain dispersed in the solvent at 300 °C, as shown in Figure 1. At first, the CdTe ends coalesce before the central CdSe

* Corresponding author. E-mail: korgel@che.utexas.edu. Tel: (512)471-5633. Fax: (512)471-7060.

10.1021/nl8015126 CCC: $40.75
Published on Web 07/11/2008

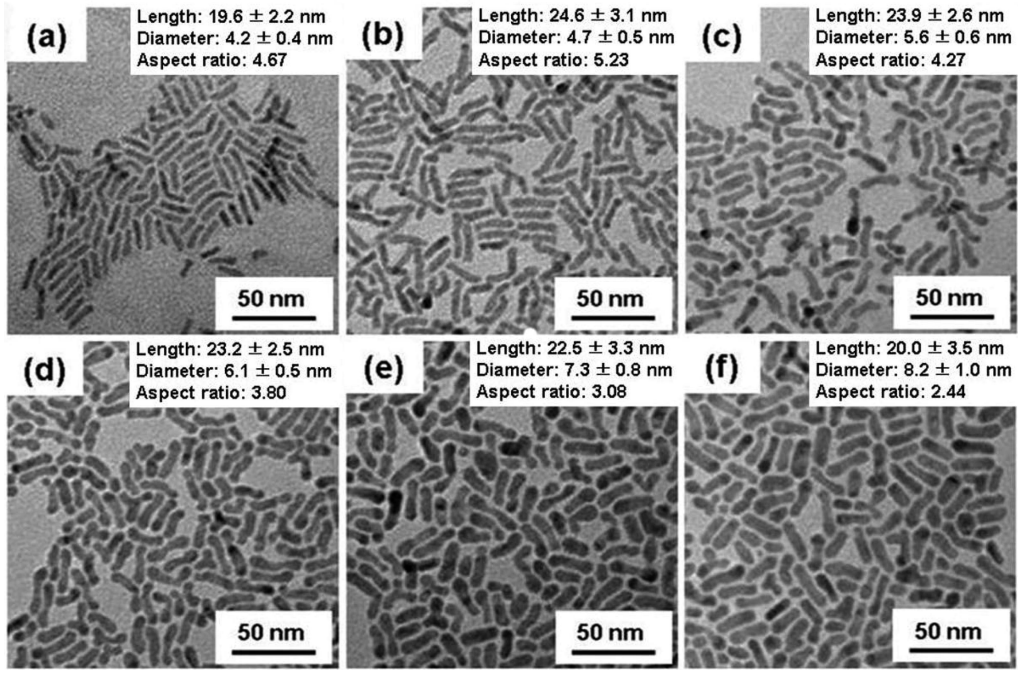

Figure 1. TEM images of (a) CdSe nanorods prior to CdTe deposition and CdTe/CdSe/CdTe heterojunction nanorods (b) immediately after CdTe deposition and then after remaining in solution at 300 °C for (c) 10 min, (d) 1 h, (e) 7 h, and (f) 30 h. The length and diameter histograms constructed from TEM images of these samples are included in the Supporting Information (Figure S3).

portion, giving the initial appearance of a dumbbell shape as has been observed previously for CdTe/CdSe/CdTe nanorods.[6–8] The nanorod diameter then becomes uniform as the nanorods continue to decrease in length. Figure 2 plots the length, radius, aspect ratio, and volume of the nanorod sample shown in Figure 1. The length decreases continuously with the coalescence rate gradually slowing as the nanorods become more spherical. The nanorod volume, however, does not remain constant (Figure 2d). There is also a slow continued deposition of CdTe (and also CdSe) from unreacted precursors as the nanorods are coalescing. To prevent this residual deposition during the aging process, nanorods were also studied that were purified after the initial CdTe deposition step and then redispersed in solution at 300 °C. Figure 3 shows TEM images of CdTe/CdSe/CdTe nanorods prepared in this way. Figure 4 shows plots of the length, radius, aspect ratio, and volume of nanorods made using this procedure. The purification largely eliminates continued CdTe deposition; however, there is still a slight increase in nanocrystal volume during aging from 800 to 1200 nm^3. It was not possible to cleanly separate the nanorods by antisolvent precipitation from unreacted precursor, but this procedure did help minimize further deposition. In both cases (with and without purification), the nanorods coalesce relatively rapidly in solution at 300 °C, with decreases in aspect ratio from just over 5 to 2 (Figure 2) and nearly 1 (Figure 4) after 30 h in solution.

The coalescence of rod-shaped nanoparticles has been examined in some detail for particles formed in aerosol (gas-phase) processes,[25,26] but such analyses have not yet been extended to nanorods in solution, even though the fundamental rate processes are identical, with coalescence to spheres being driven by the surface tension gradient on the particle surface arising from the nonspherical shape. One way to estimate the coalescence rate is to assume that continuum viscous flow applies to the nanorods and to then take mass and energy balances to obtain a relationship between the coalescence time t, and the nanorod length L, and radius r. As derived in the Supporting Information using an approach similar to that of Hawa and Zachariah, the relationships between the nanorod length and radius and coalescence time from such a continuum viscous flow model are[25]

$$t = -\frac{12\eta}{\sigma}\int_{L_0}^{L}\left(\sqrt{\frac{\pi}{V}}L^{3/2} - 2\right)^{-1} \mathrm{d}L \tag{1}$$

, and

$$t = \frac{24\eta}{\sigma}\int_{R_0}^{R}\left(1 - \frac{2\pi r^3}{V}\right)^{-1} \mathrm{d}r \tag{2}$$

In eqs 1 and 2, the nanorod volume, V, does not change with time (i.e., mass is conserved). L_0 and R_0 are the initial length and radius, respectively. The coalescence rate in this viscous flow model depends on the two materials-dependent parameters of viscosity and the surface tension, η and σ. For a fluid, η and the diffusion coefficient, D, can be related by the Eyring equation[27]

$$\eta = \frac{kT}{a_0 D} \tag{3}$$

where k is Boltzmann's constant, T is the temperature, and a_0 is the interatomic spacing. Since the nanorods are well below the melting temperatures of CdTe and CdSe, the use of eq 3 to determine η provides only an upper bound to the

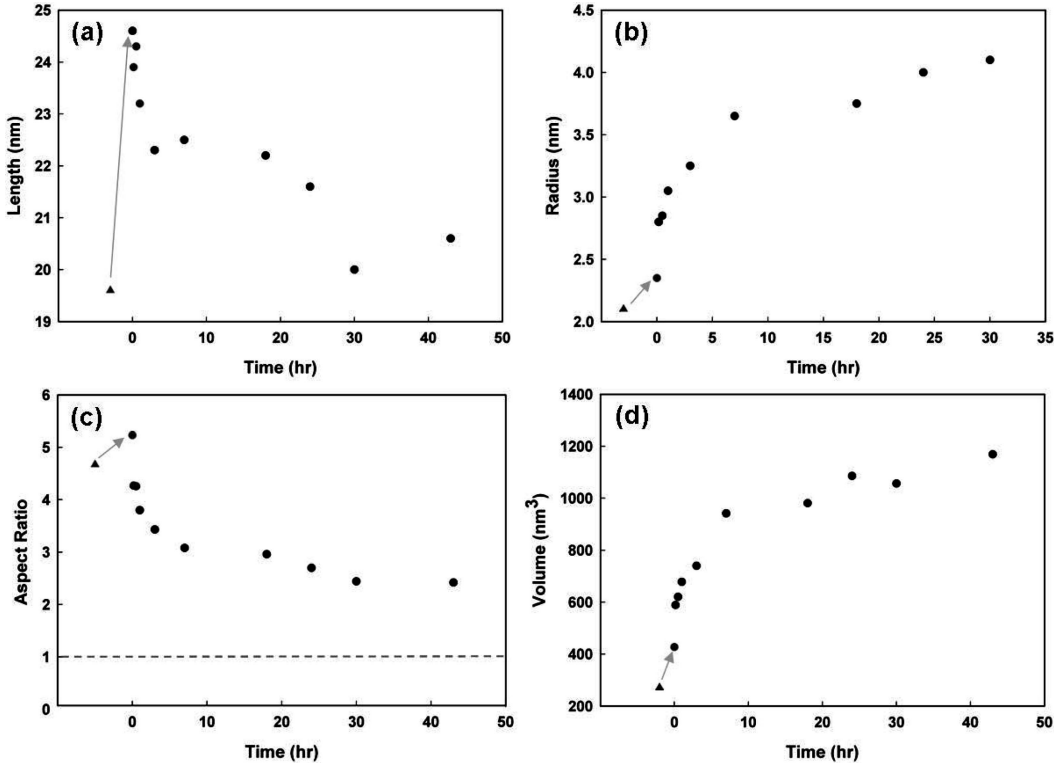

Figure 2. (a) Length, (b) radius, (c) aspect ratio, and (d) volume of CdTe/CdSe/CdTe heterojunction nanorods (determined from TEM measurements) aged in solution at 300 °C. These samples correspond to the nanorods imaged in Figure 1. The triangles correspond to the CdSe nanorods before CdTe deposition and the arrows indicate the change in dimensions immediately after Te-TOP addition to the reaction mixture. The dotted line in (c) corresponds to the aspect ratio of sphere (= 1). The (d) volume was estimated from the measured radius and length assuming a cylindrical geometry of vol = $\pi R^2 L$ (R, radius; L, length).

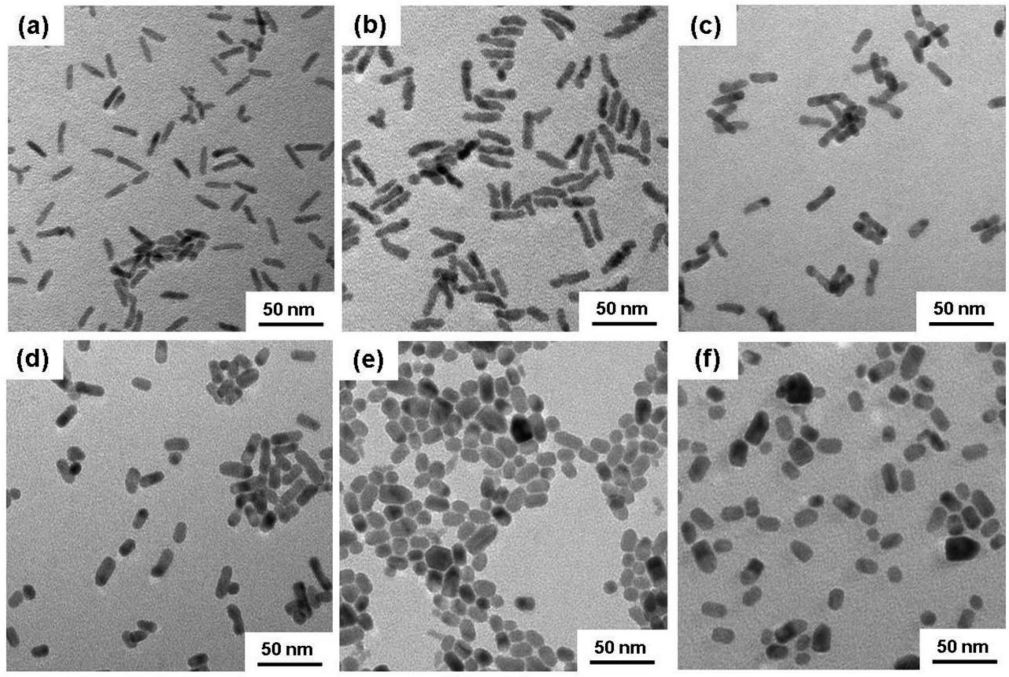

Figure 3. TEM images of CdTe/CdSe/CdTe heterojunction nanorods aged after purifying the as-formed CdTe/CdSe/CdTe nanorods prior to aging in solution at 300 °C: (a) CdSe nanorods prior to CdTe deposition; (b) CdTe/CdSe/CdTe nanorods immediately after CdTe deposition; after redispersing the CdTe/CdSe/CdTe nanorods at 300 °C for (c) 10 min, (d) 1 h, (e) 7 h, and (f) 30 h.

nanorod coalescence rate. A more accurate relationship between an effective viscosity of a crystal with a nanoscale domain size and its solid-state diffusion coefficient has been derived by Herring[28]

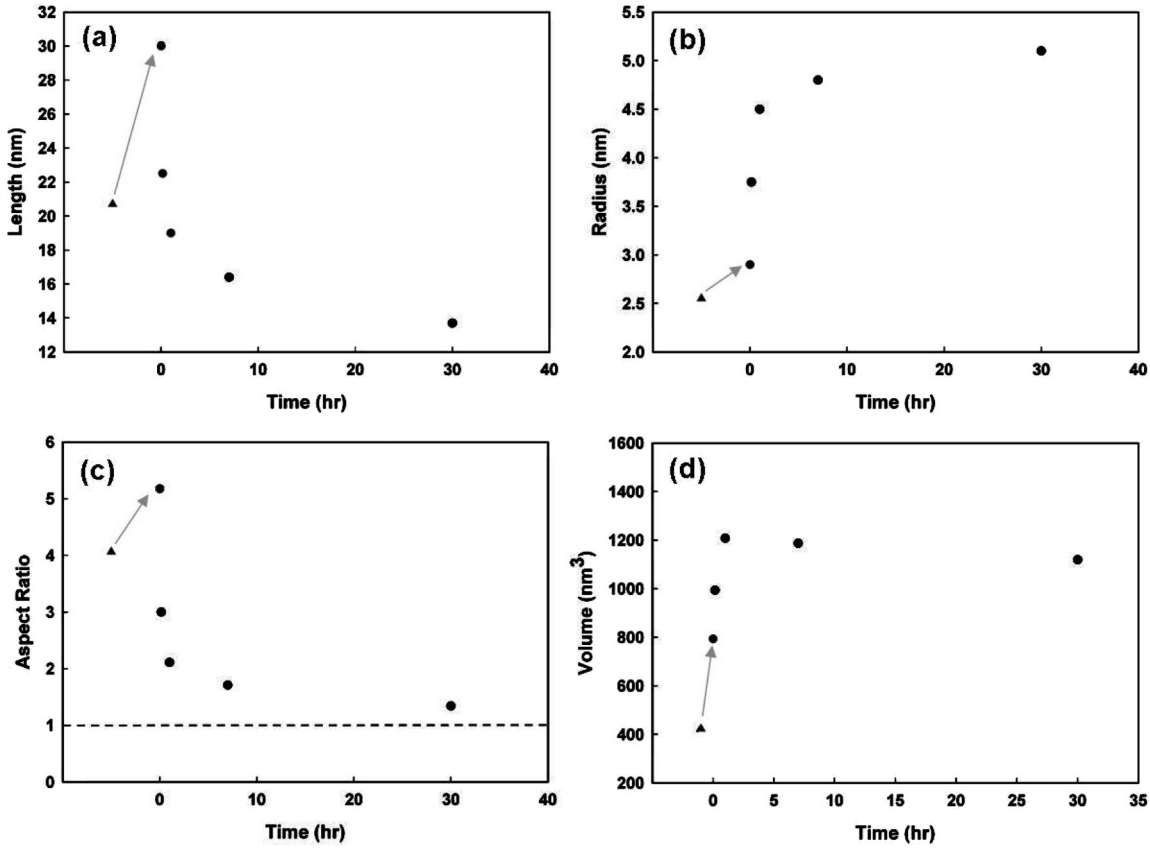

Figure 4. (a) Length, (b) radius, (c) aspect ratio, and (d) volume of CdTe/CdSe/CdTe heterojunction nanorods (determined from TEM measurements; representative images shown in Figure 3) aged in solution at 300 °C. These nanorods were subjected to a purification step immediately after the addition of the Te-TOP reactant to try to remove unreacted precursor. The triangles correspond to the CdSe nanorods before CdTe deposition and the arrows indicate the change in dimensions immediately after Te-TOP addition to the reaction mixture. The dotted line in (c) corresponds to the aspect ratio of sphere (= 1). The (*d*) volume was estimated from the measured radius and length assuming a cylindrical geometry of vol = $\pi R^2 L$ (R, radius; L, length).

$$\eta = \frac{kTR^2}{4\Omega_0 D} \tag{4}$$

In eq 4, R is the nanorod radius and Ω_0 is the atomic volume in the solid. The value of η that was determined using eq 4 is close to 2 orders of magnitude higher than η that was calculated using eq 3. The expression for η in eq 4 yields the same functional form of the coalescence frequency as that predicted by Friedlander and Wu[26] for coalescing solid particles, indicating that the use of the viscous flow model equations 1 and 2, combined with eq 4, should provide a reasonable approximation for the coalescence rate of the nanorods.

To quantitatively compare the coalescence rates predicted by eqs 1 and 2, the extra CdTe deposition on the CdTe/CdSe/CdTe nanorods that occurs during the aging process must be subtracted from the total volume of the nanorods to determine the reduction in length by coalescence. This was done by subtracting the (measured) additional particle volume from the initial CdTe/CdSe/CdTe nanorod volume and considering that the deposition rate on the ends of the nanorods is 10 times as fast as the sidewall deposition. Figure 5 plots the (corrected) nanorod length and radius as a function of aging time. The best fits of eqs 1 and 2 to the data in Figure 5 give estimates of σ/η equal to 12 and 24 nm/hr for the two different sets of experiments. These values are about an order of magnitude lower than those calculated using eq 3 and the bulk values of the CdSe surface tension and diffusion coefficient.[29] Also, the best fit values of $\sigma/\eta = 12$ nm/hr and $\sigma/\eta = 24$ nm/hr are slightly higher than the values of $\sigma/\eta = 6.4$ nm/hr and $\sigma/\eta = 4.2$ nm/hr predicted using eq 4 to estimate η.[29] Therefore, it appears that the continuum viscous flow model provides an upper bound for the coalescence rate when used in conjunction with the Eyring equation (eq 3) to relate η and D, and perhaps a lower bound for the coalescence rate when Herring's equation relating η and D (eq 4) is used.

As the nanorods age in solution at 300 °C, Se and Te interdiffusion occurs across the heterojunctions, as illustrated in Scheme 1. The interdiffusion is observable by XRD (see Supporting Information) and nanobeam energy dispersive X-ray spectroscopy (EDS) mapping (Figure 6) (see Supporting Information for additional EDS data). By measuring the rate of Te−Se interdiffusion at the heterojunctions, D for Te diffusion into CdSe can be estimated and compared to bulk values. A solution to the time-dependent diffusion equation ($\partial C/\partial t = D(\partial^2 C/\partial t^2)$) provides a relationship between the Te concentration profile and D:[33]

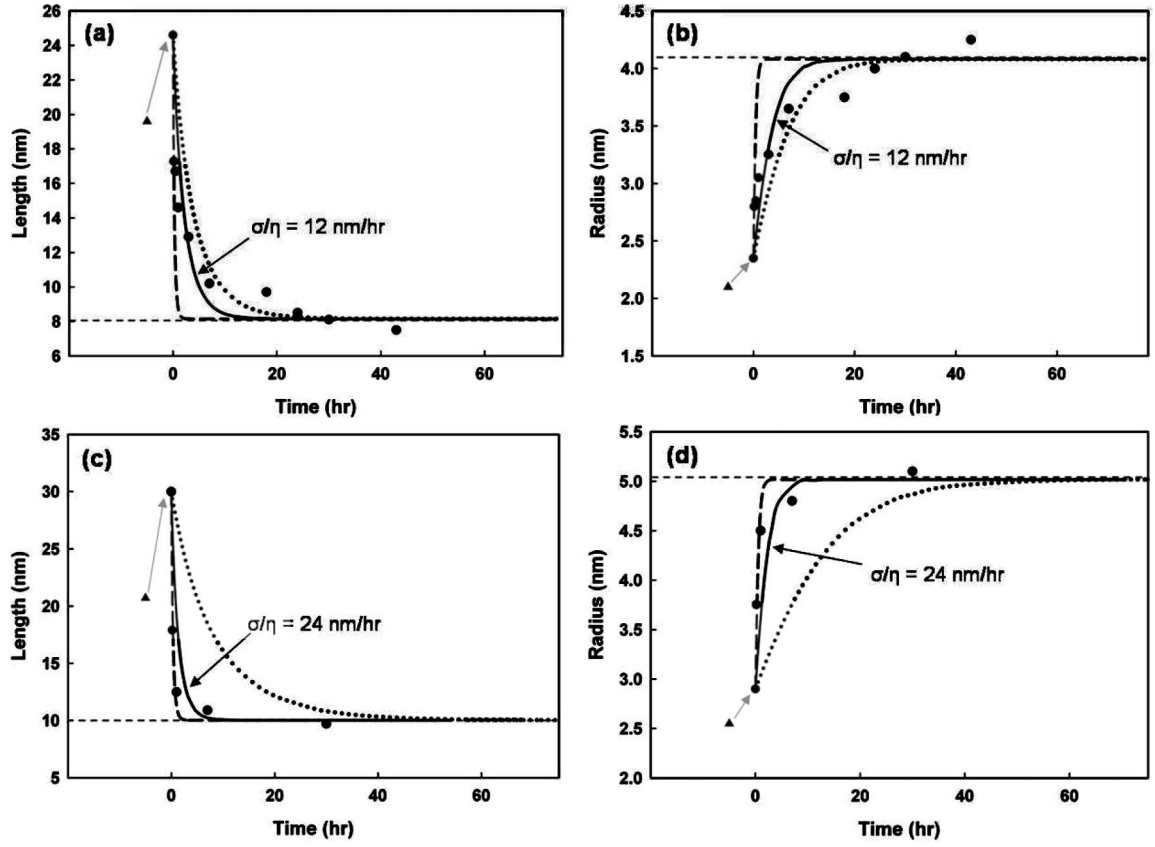

Figure 5. Corrected (a,c) length and (b,d) radius versus aging time (solid dots) in TOP/TOPO solution at 300 °C and model predictions using eqs 1 and 2 (solid, dashed, and dotted lines). The data in panels a and b correspond to the nanorod samples imaged in Figure 1, and the data in panels c and d correspond to the "purified" nanorod samples imaged in Figure 3. The dashed and dotted curves in panels a−d are plots of eqs 1 and 2 calculated using eqs 3 and 4, respectively, to determine η. The use of bulk values of D, σ, Ω_0, a_0, and averaged values of R gave $\sigma/\eta = 96$ nm/hr (dashed curves) using eq 3 and $\sigma/\eta = 6.4$ nm/hr (dotted curves in panels a and b) and $\sigma/\eta = 4.2$ nm/hr (dotted curves in panels c and d) using eq 4.[29] The solid curves are the best fits of eqs 1 and 2 to the data. The horizontal dotted lines indicate the nanorod lengths and radii for spherical particles with the same volume as the starting nanorods (i.e., the final limiting condition when the aspect ratio equals 1).

Scheme 1. Se and Te Interdiffusion at the CdSe/CdTe Interfaces Leads To Transformation of CdTe/CdSe/CdTe Heterojunction Nanorods Into Alloyed CdSeTe Nanoparticles

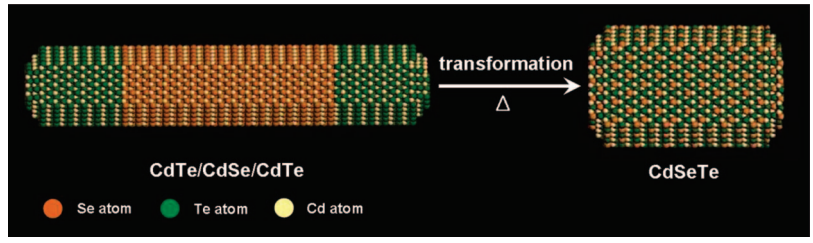

$$C(x,t) = \frac{Q}{\sqrt{\pi Dt}} \exp\left(-\frac{x^2}{4Dt}\right) \quad (5)$$

In eq 5, x is the distance from the end of the rod, t is the aging time and Q is the amount of CdTe initially deposited at the end of the nanorod. Therefore, D can be estimated by determining the diffusion length, $l = \sqrt{Dt}$, which is the position at which the Te concentration decreased to $1/e$ the value of the peak concentration, as a function of aging time.[33–35] From EDS data like that shown in Figure 6, l was determined for four different nanorods at four different aging times (see Supporting Information for additional EDS data and the procedure used for determining l). Performing the elemental maps on each nanorod is a relatively time intensive process and it is not practical to measure tens or hundreds of nanorods; however, elemental maps of four nanorods at each aging time were obtained and averaged to minimize the error in l as much as possible. Figure 7 shows a plot of l^2 versus the aging time, showing a linear dependence that indicates that strain at the CdTe/CdSe interface (see Supporting Information) is not affecting D.[34,35] A linear curve fit to the data in Figure 7 gives a value of $D = 1.5 \times 10^{-17}$ cm^2/sec, which is close to the literature value[30] of 2×10^{-17} cm^2/sec.

In summary, both coalescence and Te−Se interdiffusion occur as CdTe/CdSe/CdTe nanorods are aged in solution at 300 °C. The rates of Se−Te interdiffusion and nanorod

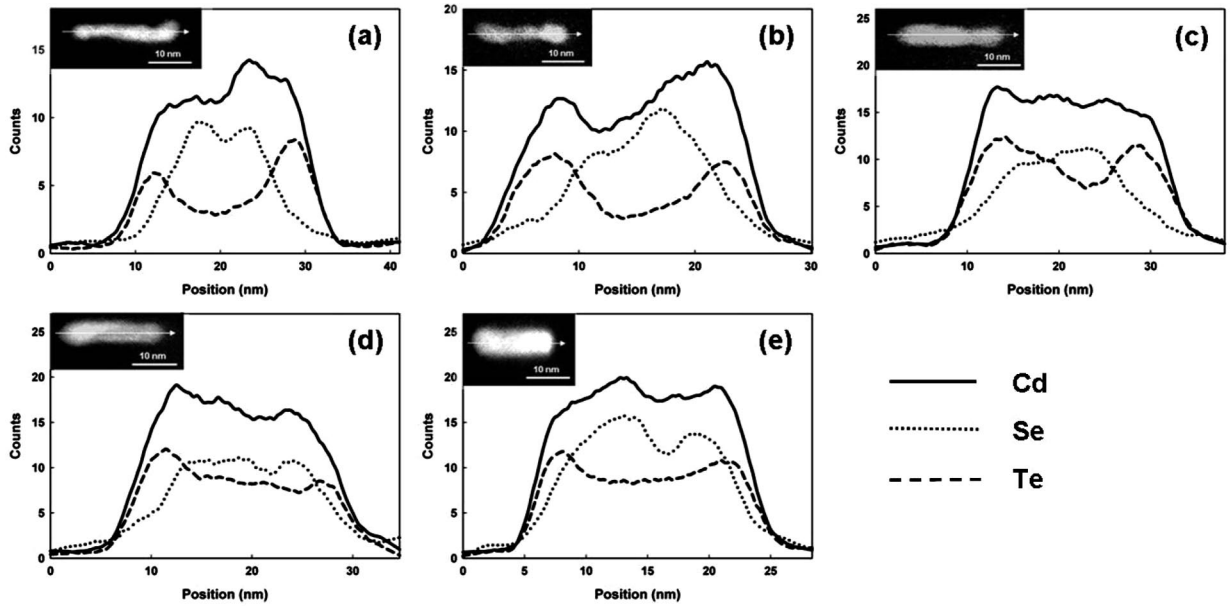

Figure 6. Cd, Se, and Te composition profiles measured by nanobeam EDS down the length of individual CdTe/CdSe/CdTe heterostructure nanorods (a) immediately after CdTe deposition at the ends of the CdSe nanorods, and after aging in solution at 300 °C for (b) 10 min, (c) 1 h, (d) 7 h, and (e) 30 h. (Insets) Dark-field STEM images of the corresponding nanorods. The arrow indicates the line scan direction. The undulations in the concentration profiles result from slight fluctuations in nanorod diameter along the nanorod length.

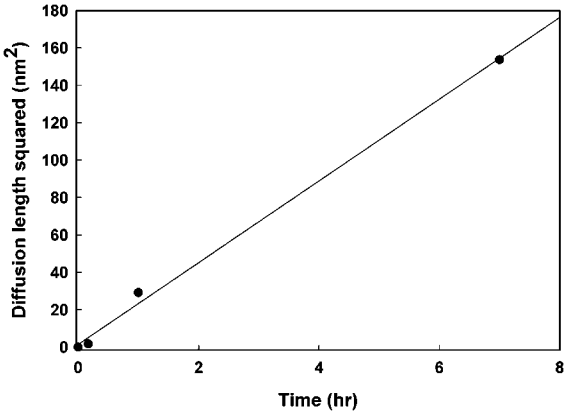

Figure 7. Plot of the square of the Te diffusion length measured by EDS mapping versus aging time. D estimated from a linear fit of the data to eq 5 is 1.5×10^{-17} cm^2/sec. (Each point on the plot is a diffusion length averaged for four different nanorods; see Supporting Information for Details.)

coalescence were measured. Although there is strain at the epitaxial CdTe/CdSe interface due to the lattice mismatch, this strain does not appear to influence the rate of Te−Se interdiffusion. A continuum viscous flow model provided a reasonable approximation of the measured coalescence rates. Nonetheless, there are many questions that remain to be answered about the coalescence rate of nonspherical nanocrystals, which require more accurate predictive models for coalescence that can be compared directly to experimental measurements such as these. For example, how significantly do the capping ligands influence the coalescence rates? The adsorbed capping ligands should lower the nanocrystal surface tension,[36] which should in turn slow the coalescence rate. The role of the ligands in slowing nanorod coalescence could be particularly influential in situations in which nanocrystals aggregate into linear chains, as in the oriented attachment mechanism.[37,38] In the case of the CdTe/CdSe/CdTe nanorods studied here, the phosphonic acid ligands adsorb more strongly to the nonpolar side facets than the polar surfaces at the ends of the nanorods,[39,40] which may further stabilize the rod shape by lowering the surface tension on specific crystal facets. More accurate, predictive models of chemical and physical transformations in nanocrystals, such as the coalescence and atomic interdiffusion studied here, are needed; however, it appears that relatively simple continuum models can nevertheless provide some rough guidelines for how fast these processes occur.

Acknowledgment. This research was supported in part by funding from the National Science Foundation through their STC program (CHE-9876674), the Robert A. Welch Foundation, the Advanced Prototype and Processing Center (AP2C: DARPA HR00011-06-1-0005), the Office of Naval Research (N000N-05-1-0857), and the Air Force Research Laboratory (FA8650-07-2-5061).

Supporting Information Available: Experimental details, XRD data, nanorod-sizing histograms, derivation of the continuum viscous flow model of a coalescing nanorod, coalescence rate plots at various values of σ/η, additional nanobeam EDS line scans, determination of the Te diffusion length by EDS, and high resolution TEM images of a CdTe/CdSe interface. This material is available free of charge via the Internet at http://pubs.acs.org.

References

(1) Mews, A.; Eychmueller, A.; Giersig, M.; Schooss, D.; Weller, H. *J. Phys. Chem.* **1994**, *98*, 934.
(2) Kamalov, V. F.; Little, R.; Logunov, S. L.; El-Sayed, M. A. *J. Phys. Chem.* **1996**, *100*, 6381–6384.

(3) Dorfs, D.; Eychmuller, A. *Z. Phys. Chem.* **2006**, *220*, 1539–1552.
(4) Manna, L.; Scher, E. C.; Li, L.-S.; Alivisatos, A. P. *J. Am. Chem. Soc.* **2002**, *124*, 7136.
(5) Mokari, T.; Rothenberg, E.; Popov, I.; Costi, R.; Banin, U. *Science* **2004**, *304*, 1787.
(6) Shieh, F.; Saunders, A. E.; Korgel, B. A. *J. Phys. Chem. B.* **2005**, *109*, 8538.
(7) Halpert, J. E.; Porter, V. J.; Zimmer, J. P.; Bawendi, M. G. *J. Am. Chem. Soc.* **2006**, *128*, 12590.
(8) Kumar, S.; Jones, M.; Lo, S. S.; Scholes, G. D. *Small* **2007**, *3*, 1633.
(9) Jones, M.; Kumar, S.; Lo, S. S.; Scholes, G. D. *J. Phys. Chem. C* **2008**, *112*, 5423–5431.
(10) Milliron, D. J.; Hughes, S. M.; Cui, Y.; Manna, L.; Li, J. B.; Wang, L. W.; Alivisatos, A. P. *Nature* **2004**, *430*, 190.
(11) Yong, K. T.; Sahoo, Y.; Swihart, M. T.; Prasad, P. N. *Adv. Mater.* **2006**, *18*, 1978.
(12) Robinson, R. D.; Sadtler, B.; Demchenko, D. O.; Erdonmez, C. K.; Wang, L.-W.; Alivisatos, A. P. *Science* **2007**, *317*, 355–358.
(13) Coe, S.; Woo, W. K.; Bawendi, M.; Bulovic, V. *Nature* **2002**, *420*, 800–803.
(14) Zhong, H.; Zhou, Y.; Yang, Y.; Yang, C.; Li, Y. *J. Phys. Chem. C.* **2007**, *111*, 6538.
(15) Konstantatos, G.; Howard, I.; Fischer, A.; Hoogland, S.; Clifford, J.; Klem, E.; Levina, L.; Sargent, E. H. *Nature* **2006**, *442*, 180–183.
(16) Chen, X.; Lou, Y.; Samia, A. C.; Burda, C. *Nano Lett.* **2003**, *3*, 799.
(17) Shenoy, V. B. *Phys. Rev. B* **2005**, *71*, 094104.
(18) Dingreville, R.; Qu, J. M.; Cherkaoui, M. *J. Mech. Phys. Solids* **2005**, *53*, 1827–1854.
(19) Wang, Y.; Cai, L.; Xia, Y. *Adv. Mater.* **2005**, *17*, 473.
(20) Peng, S.; Sun, S. *Angew. Chem., Int. Ed.* **2007**, *46*, 4155.
(21) Yin, Y.; Erdonmez, C. K.; Cabot, A.; Hughes, S.; Alivisatos, A. P. *Adv. Funct. Mater.* **2006**, *16*, 1389.
(22) Puntes, V. F.; Krishnan, K. M.; Alivisatos, A. P. *Science* **2001**, *291*, 2115.
(23) Jun, Y.-w.; Jung, Y.-y.; Cheon, J. *J. Am. Chem. Soc.* **2002**, *124*, 615.
(24) Saunders, A. E.; Koo, B.; Wang, X.; Shih, C.-K.; Korgel, B. A. *ChemPhysChem.* **2008**, *9*, 1158–1163.
(25) Hawa, T.; Zachariah, M. R. *Phys. Rev. B* **2007**, *76*, 054109.
(26) Friedlander, S. K.; Wu, M. K. *Phys. Rev. B* **1994**, *49*, 3622–3624.
(27) Glasstone, S.; Laidler, K. J.; Eyring, H. *The Theory of Rate Processes*; McGraw-Hill: New York, 1941.
(28) Herring, C. *J. Appl. Phys.* **1950**, *21*, 437–445.
(29) For the calculations, values of $D = 2 \times 10^{-17}$ cm^2/sec (Te into CdSe),[30] $\sigma = 0.5$ J/m^2,[31,32] $\Omega_o = 0.0547$ nm^3, $a_o = 2.8 \times 10^{-10}$ m, and averaged R values of 3.4 and 4.2 nm for eq 4 were used.
(30) Kokkonis, P.; Leute, V. *Solid State Ionics* **2005**, *176*, 2681.
(31) Balasubramanian, R.; Wilcox, W. R. *Int. J. Thermophysics* **1990**, *11*, 25.
(32) Kumikov, V. K.; Khokonov, Kh. B. *J. Appl. Phys.* **1983**, *54*, 1346.
(33) Plummer, J. D.; Deal, M. D.; Griffin, P. B. *Silicon VLSI Technology: Fundamentals, Practice and Modeling*; Prentice Hall: Upper Saddle River, NJ, 2000.
(34) Khreis, O. M. *Solid State Commun.* **2004**, *132*, 767.
(35) Gillin, W. P.; Dunstan, D. J. *Phys. Rev. B* **1994**, *50*, 7495.
(36) Leff, D. V.; Ohara, P. C.; Heath, J. R.; Gelbart, W. M. *J. Phys. Chem.* **1995**, *99*, 7036.
(37) Tang, Y. Z.; Kotov, N. A.; Giergsig, M. *Science* **2002**, *297*, 237–240.
(38) Cho, K. S.; Talapin, D. V.; Gaschler, W.; Murray, C. B. *J. Am. Chem. Soc.* **2005**, *127*, 7140–7147.
(39) Nair, P. S.; Fritz, K. P.; Scholes, G. D. *Small* **2007**, *3*, 481–487.
(40) Puzder, A.; Williamson, A. J.; Zaitseva, N.; Galli, G.; Manna, L.; Alivisatos, A. P. *Nano Lett.* **2004**, *4*, 2361–2365.

NL8015126